PNAS RESEARCH ARTICLE | PHARMACOLOGY OPEN ACCESS

Next-generation rifamycins for the treatment of mycobacterial infections

Véronique Dartois[a,b,1], Tian Lan[c], Uday S. Ganapathy[a,b], Chui Fann Wong[a], Jickky P. Sarathy[a], Diana C. Jimenez[d], Ilham M. Alshiraihi[d], Ha Lam[d], Suyapa Rodriguez[a], Min Xie[a], Maritza Soto-Ojeda[d], Mary Jackson[d], William Wheat[d], Nathan C. Dillman[c], Kateryna Kostenkova[c], Jake Schmitt[c], Lea Mann[e], Adrian Richter[e], Peter Imming[e], Jansy Sarathy[a,b], Firat Kaya[a], Sindhuja Paruchuri[a], Betelhem Tatek[a], Camilla Folvar[a], Julianna Proietto[a], Matthew Zimmerman[a], Mercedes Gonzalez-Juarrero[d], Courtney C. Aldrich[c], and Thomas Dick[a,b,f]

Affiliations are included on p. 8.

Edited by William Jacobs Jr., Albert Einstein College of Medicine, Bronx, NY; received November 15, 2024; accepted February 18, 2025

***Mycobacterium abscessus* is a rapidly growing nontuberculous *Mycobacterium* causing severe pulmonary infections, especially in immunocompromised individuals and patients with underlying lung conditions like cystic fibrosis (CF). While rifamycins are the pillar of tuberculosis treatment, their efficacy against *M. abscessus* lung disease is severely compromised by intrabacterial ADP-ribosylation. Additionally, rifamycins induce cytochrome P450 3A4 (CYP3A4), a major human drug-metabolizing enzyme, further limiting their use in patients with comorbidities that require treatment with CYP3A4 substrates such as CF and HIV coinfection. We chemically reengineered rifabutin to enhance its potency against *M. abscessus* by blocking intrabacterial inactivation and eliminate drug–drug interactions by removing induction of CYP3A4 gene expression. We have designed and profiled a series of C25-substituted derivatives resistant to intracellular inactivation and lacking CYP3A4 induction, while retaining excellent pharmacological properties. Against *Mycobacterium tuberculosis*, devoid of ADP-ribosyltransferase, the frontrunners are equipotent to rifabutin, suggesting superior clinical utility since they no longer come with the drug interaction liability typical of rifamycins. Prioritized compounds demonstrated superior antibacterial activity against a panel of *M. abscessus* clinical isolates, were highly bactericidal against replicating and drug-tolerant nonreplicating bacteria in caseum surrogate and were active against intracellular bacteria. As single agents, these rifamycins were as effective as a standard-of-care four-drug combination in a murine model of *M. abscessus* lung infection.**

rifamycin | drug discovery | *Mycobacterium abscessus* | pulmonary infection | preclinical development candidate

Significance

Mycobacterium abscessus lung disease is a growing global health crisis due to limited therapeutic options and emerging drug-resistant strains. To address this unmet clinical need, we are developing oral rifamycins with enhanced antibacterial potency, reduced drug–drug interactions, and improved pharmacological properties. Their superior efficacy in a mouse model of infection underscores their therapeutic potential to cure *M. abscessus* lung disease. The preclinical candidates described here will advance to IND (investigational new drug)-enabling studies to support clinical development. These rifamycins may also find clinical utility for the treatment of TB-HIV and lung disease caused by other NTM pathogens. This is a successful drug discovery program delivering 2nd generation rifamycins with improved efficacy specifically against mycobacterial infections.

Rifamycins, targeting the RNA polymerase, are the pillars of antituberculosis (TB) therapy. They achieve potent sterilizing activity against heterogenous mycobacterial populations and display favorable penetration to the site of disease (1, 2). They inhibit a clinically validated target and have excellent oral bioavailability, tolerability, and efficacy history. When introduced in the 1960s, rifampicin contributed to reducing therapy duration from 24 to 6 mo (3). Rifabutin (RBT) is substituted for rifampicin in patients with comorbidities requiring treatment with CYP3A4 substrates such as antiretroviral protease inhibitors because it is a weaker inducer of CYP3A4 (4). Rifapentine is part of the first 4-mo drug regimen ever shown to be noninferior to the 6-mo standard of care (5) and is included in the preferred and shortest regimens for the prevention of latent TB reactivation as daily and once-weekly combinations with isoniazid (6). Thus, three rifamycins are at the center stage of TB therapy and treatment shortening. Yet, this has not translated into similar clinical utility against pulmonary disease caused by *Mycobacterium abscessus* (Mab-PD), a related nontuberculous mycobacterial infection intrinsically resistant to many antibiotic classes (7).

Rifamycins suffer from two intrinsic resistance pathways due to intrabacterial metabolism across mycobacteria: oxidation and ADP-ribosylation. We have shown that rifamycins containing the less readily oxidizable naphthoquinone core such as RBT are more potent than naphthohydroquinone-containing analogs such as rifampicin, because they cannot be inactivated by mycobacterial monooxygenases (8, 9). All rifamycins inhibit and kill bacteria via binding to DNA-dependent RNA polymerase (RNAP), primarily mediated by C1-, 8-, 21-, and 23-OH groups (10). Mab prevents this interaction by ADP-ribosylation of rifamycins at C23. The responsible bacterial ADP-ribosyltransferase (Arr) is present in many bacterial species (11) and transfers an ADP-ribosyl group from NAD^+ to C23-OH, thus blocking rifamycin binding to RNAP. Deletion of the Arr-encoding gene overcomes intrinsic rifamycin resistance of *Mycobacterium smegmatis* (12) and Mab (8, 13). We and others have

Competing interest statement: PCT/US2023/034573 (16).

This article is a PNAS Direct Submission.

[1]To whom correspondence may be addressed. Email: veronique.dartois@hmh-cdi.org.

This article contains supporting information online at https://www.pnas.org/lookup/suppl/doi:10.1073/pnas.2423842122/-/DCSupplemental.

Published May 1, 2025.

shown that modifications at the C25 position with a carbamate group on 3-morpholino rifamycin SV (14) or with a bulkier ester group on RBT (15, 16) blocks enzymatic inactivation by Arr_{Mab} while maintaining binding to the RNAP target, in line with our screens of archived rifamycin collections against Mab (8). Following this medicinal chemistry rationale, we have designed RBT analogs that overcome intrabacterial ribosylation and generated molecules with 20- to 100-fold increased potency against Mab (15).

The clinical utility of rifamycins for Mab-PD patients who suffer from comorbidities critically depends on minimizing or suppressing drug–drug interactions with CYP3A4 substrates. For instance, the cystic fibrosis (CF) transmembrane conductance regulator (CFTR) modulators have changed the life of people with CF (17), but are metabolized by CYP3A4 (18). Likewise, most protease inhibitors and nonnucleoside reverse transcriptase inhibitors used in the treatment of people with HIV are CYP3A4 substrates. This precludes (in people with CF) or limits (in people with HIV) treatment of bacterial infections with currently approved rifamycins, including RBT despite its reduced potential for CYP3A4 induction compared to rifampicin (19). Thus, removing the CYP3A4 induction liability while maintaining potency and attractive pharmacokinetics (PK) is critical for the treatment of Mab-PD (20).

Here, we describe the in vitro and in vivo PK, pharmacodynamics (PD) and mouse efficacy of six frontrunners that have emerged from a collaborative lead optimization program. Using the GM-CSF knockout (KO) mouse model of acute Mab infection (21, 22), we show that reduction of bacterial burden in the lungs correlates with standard PK-PD parameters. Selecting analogs that ranked highest in a mouse model of acute Mab infection and did not induce CYP3A4 mRNA expression more than twofold at 1 μM delivered two preclinical development candidates (PDC) that approach apparent sterilization of mouse lungs after 7 d of daily oral administration.

Results

Screening and Progression Cascade for the Discovery of Efficacious Rifamycins against Mab-PD. The preclinical and clinical efficacy of rifamycins is driven by the ratio between the drug concentration over time in plasma or area under the concentration-time curve (AUC), and the minimum inhibitory concentration (MIC). At the clinical dose of 300 mg daily, the AUC/MIC_{Mtb} (MIC against *M. tuberculosis* Mtb) ratio of RBT is around 500 to 600 (23, 24). Using the MIC of RBT against the Mab ATCC19977 reference strain, the AUC/MIC_{Mab} of RBT is approximately 2 to 3, thus >100-fold lower than its AUC/MIC_{Mtb}. Since RBT is successfully used in the treatment of TB and replaces rifampicin in patients coinfected with HIV, we reasoned that achieving Mtb-like PK-PD parameters would deliver efficacious rifamycins against Mab lung infections. We expanded structure-based optimization efforts that had focused on the redesign of rifamycins to block ADP-ribosylation while preserving on-target activity (15). Our objectives were to maintain potency while further improving PK properties and eliminating CYP3A4 induction. The progression cascade started with a potency screen against wild type (WT) Mab ATCC19977 and the isogenic Δ*arr* mutant to ensure that ADP-ribosylation was effectively blocked. Rifamycins that met the predefined criteria of $MIC_{WT}/MIC_{\Delta arr} < 1.5$ and $MIC_{WT} < 0.05$ μM were retained for plasma protein binding (PPB) determination, mouse PK and macrophage uptake as an indicator of distribution into cellular lung lesions. Among these, compounds that displayed total and unbound AUC/MIC at least as attractive as RBT's AUC/MIC against Mtb were shortlisted and consideration was given to macrophage uptake to select a subset with a diverse balance of plasma versus tissue PK. Six rifamycins progressed to mouse efficacy and CYP3A4 induction measurements, with RBT as the comparator (Fig. 1).

Pharmacokinetic and Pharmacodynamic Filtering for Efficacy Studies. The rifamycin analogs displayed a range of moderate to high PPB, distributed above and below RBT's PPB and generally reflective of cLogP (Fig. 2*A* and Table 1). Among the 83 analogs that were profiled for PPB, 36 were chosen for mouse PK evaluation, covering a range of acceptable fraction unbound (f_u) with considerations of physicochemical properties and chemical diversity. Remarkably, most analogs (31/36) achieved oral exposure similar or greater than RBT. Only 5 rifamycins had an oral AUC more than twofold lower than RBT, and this was

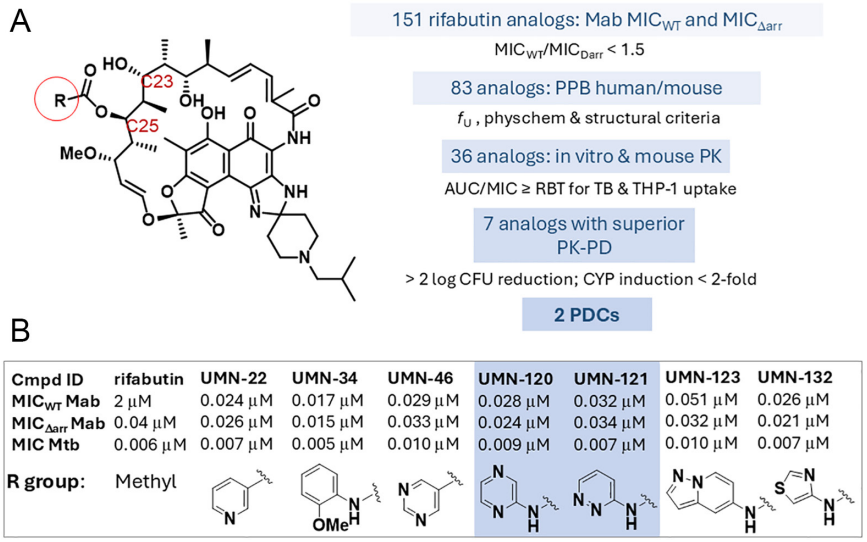

Fig. 1. Rifamycin screening cascade and optimized leads. (*A*) *Left*: rifabutin scaffold showing the C23 position where ADP-ribosylation occurs and the C25 position where substituents are introduced to block Arr-mediated ribosylation. *Right*: screening and compound profiling cascade including threshold metrics. PPB: plasma protein binding, f_u: fraction unbound; AUC: area under the concentration–time curve; PDCs: preclinical development candidates. (*B*) Potency and C25 substituents of the six selected leads that meet pharmacokinetic–pharmacodynamic criteria. MICs (concentrations that inhibit 90% growth) against the wild-type Mab reference strain ATCC19977 (MIC_{WT}) and isogenic Δ*arr* knockout strain ($MIC_{\Delta arr}$). UMN-22 and UMN-46 are referred to as **5m** and **5n** in ref. 15, respectively

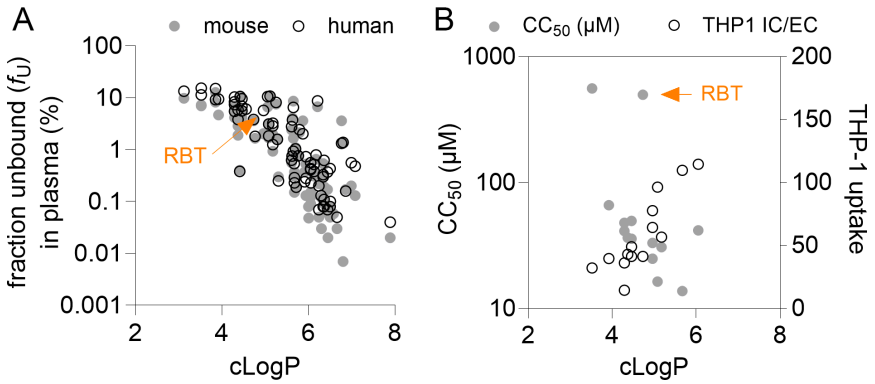

Fig. 2. Impact of cLogP on in vitro PK parameters and cytotoxicity. (*A*) cLogP versus unbound fraction (f_u) in mouse and human plasma for the series of RBT analogs. (*B*) Impact of cLogP on uptake into THP-1 macrophages and concentration that induces 50% HepG2 cell death (CC_{50}).

associated with high clearance, high volume of distribution and high hydrophobicity (cLogP 5.06 to 6.77) (Dataset S1). Next, we calculated PK-PD parameters to determine how these would compare to PK-PD metrics of RBT for TB, and to prioritize the most attractive compounds for in vivo efficacy studies. Excluding the five compounds with poor oral exposure, the AUC/MIC at 10 mg/kg (the human equivalent dose of RBT) ranged from 100 to 2,400 (Dataset S1 and *SI Appendix*, Fig. S1).

To account for PPB when calculating AUC/MIC, one may either correct the AUC for the fraction unbound (*f*AUC) or measure the MIC in the presence of 50% human serum to generate serum-shifted MIC (ssMIC). Depending on the compound class, the two methods do not always deliver similar results. The discrepancy has been attributed to differences between static and dynamic free fractions (25, 26). Thus, we measured the ssMIC of compounds that appeared promising by measure of AUC/MIC and displayed a wide range of *f*AUC/MIC. We found that the ssMIC increased as f_u decreased, but not proportionally so (Table 2) and therefore *f*AUC/MIC provided a different compound ranking than AUC/ssMIC (Table 1 and Dataset S1). Overall, the rifamycins' MIC was markedly less serum-shifted than would have been predicted based on their plasma f_u, as reflected by the inferred "active" fraction consistently higher than the f_u (Table 2). This suggests that the dynamic free fraction (26) of rifamycins is higher than their f_u and that *f*AUC/MIC may not be an adequate PK-PD index for the rifamycin class. OPC-167832 [Quabodepistat, a drug candidate in clinical trial for TB (27)], which we used as control, exhibited a serum shift of 147 proportional to its plasma f_u of ~1% as published previously (28), and consistent with its lack of efficacy in a Mab mouse model (29).

As an indicator of penetration into cellular lung lesions where Mab bacilli reside (30, 31), we measured rifamycin uptake into THP-1 derived macrophages. This was accomplished for a subset of compounds with attractive PK-PD parameters and covering a representative range of cLogP. As expected, uptake into macrophages was broadly correlated with cLogP (Fig. 2*B*). The results were considered side-by-side with the three measures of AUC/MIC (uncorrected, *f*AUC/MIC, and AUC/ssMIC) to select seven rifamycins featured in Table 1 for further biological profiling, in vitro metabolism and drug interaction assays, cytotoxicity, and mouse efficacy. Among these, five ranked highest by AUC/MIC. UMN-34 and UMN-123 were included as analogs with slightly inferior plasma PK-PD but high accumulation in macrophages (Table 1 and Dataset S1), to determine whether efficacy is primarily driven by plasma PK-PD (total or corrected for nonspecific binding) or intracellular concentrations in macrophages.

Biological Profiling of Selected Leads. To gauge the bactericidal and growth inhibitory activity of the selected leads against bacterial subpopulations found at the site of disease, we subjected them to four in vitro assays targeting extracellular, intracellular, replicating, and nonreplicating Mab bacteria. For all compounds tested, the minimum bactericidal activity (MBC_{90}, 1-log kill) in replicating cultures was within twofold the MIC, as is commonly observed for the rifamycin class and previously observed for RBT (32). Concentration-kill curves against nonreplicating persisters in caseum surrogate showed remarkable dose–response activity given the profound drug tolerance of these bacteria (2) (Fig. 3*A* and *SI Appendix*, Fig. S2). UMN-34 was less potent than the others, potentially due to its very high nonspecific binding to macromolecules (Table 1). Against intracellular Mab ATCC19977 in THP-1 macrophages, the IC_{50}s were in the same range as MICs. Compounds with higher partitioning into THP-1 cells were slightly more potent (Table 1 and *SI Appendix*, Fig. S3). Finally, we measured the bactericidal activity of the rifamycins against intracellular Mab in macrophages at 1 and 10 μM, spanning the concentration range achieved in mouse plasma at the projected efficacious dose. At these concentrations, RBT did not inhibit intracellular growth of Mab. All UMN compounds were bactericidal, significantly reducing the intracellular burden compared to the start of treatment, even at the lower concentration (Fig. 3*B*). Although bactericidal activity was not proportional to uptake in THP-1 cells across the series (Table 1), the most potent compound UMN-34 also exhibits the highest partitioning into macrophages, indicating that high uptake may contribute to superior activity but that other factors are at play.

In Vitro PK, Metabolism, and Cytotoxicity. To understand the CYP3A4 induction potential of the series compared to RBT, a subset of 15 analogs were selected and their impact on CYP3A4 mRNA expression was quantified in human hepatocytes, compared to RBT which induces mRNA expression by 33 and 43-fold at 1 and 10 μM, respectively. All C25-substituted rifamycins caused reduced CYP3A4 induction compared to RBT, ranging from onefold to ninefold at 1 μM and 1 to 14-fold at 10 μM (Table 1 and Dataset S1). These findings suggest that the chemical modifications at C25 interfere with rifamycin binding to the human pregnane X receptor (PXR) that activates CYP3A4 transcription. Four of the selected leads induced CYP3A4 mRNA expression by less than twofold at 1 μM, qualifying them as noninducers according to FDA guidance (33). This prompted us to measure their MIC against *M. tuberculosis* to assess their potential utility for TB patients receiving CYP3A4 substrates either as TB antibiotics or to treat other indications such as HIV infection. We found

Table 1. Pharmacokinetic and pharmacodynamic parameters of optimized leads

	RBT	UMN22	UMN34	UMN46	UMN120	UMN121	UMN123	UMN132
Potency*								
WT Mab MIC (μM)	2.0	0.024	0.017	0.029	0.028	0.035	0.051	0.026
Δ*arr* Mab MIC (μM)	0.04	0.026	0.015	0.033	0.024	0.031	0.032	0.021
$ssMIC_{50}$ Mab (μM)	2.5	0.15	0.15	0.048	0.045	0.26	0.14	0.05
MBC_{90} (μM)	3.5	0.05	n.d.	n.d.	0.05	0.06	n.d.	n.d.
Mtb MIC (μM)	0.006	0.007	0.005	0.010	0.009	0.007	0.010	0.007
$MacIC_{50}$ (μM)	0.7	0.03	0.01	n.d.	0.03	0.04	0.01	0.01
$CasMBC_{90}$ (μM)	72	2	20	0.7	1.3	0.5	1.0	0.5
Caseum f_u (%)	0.94	0.39	0.006	1.18	0.66	0.96	0.05	0.17
In vivo pharmacokinetics and PK-PD								
V_d (L/kg)	3.9	1.8	4.5	2.4	0.8	0.5	1.1	1.5
CL (mL/kg*h)	619	179	220	235	132	136	151	148
Elimination $t_{1/2}$ (h)	4.3	6.7	14.1	7.2	4.0	2.5	5.2	6.8
Average AUC at 10 mg/kg (ng*h/mL, n = 3)	11,179	43,875	11,283	33,948	55,072	40,339	29,529	35,699
Bioavailability (%)	69.2	78.7	22.4	79.9	73.6	56.2	44.6	52.7
AUC/MIC @ 10 mg/kg	5.6	2,194	752	1,886	1,967	1,180	579	1,373
*f*AUC/MIC at 10 mg/kg	0.2	50	1	96	89	64	2	25
AUC/ssMIC @ 10 mg/kg	4.7	293	68	707	1224	125	211	714
AUC/ssMIC @ efficacious dose	65	984	292	n.d.	2,572	920	230	859
In vitro pharmacokinetics								
MW	847.02	910.08	954.13	911.07	926.08	926.08	964.12	931.12
ClogP†	4.73	4.96	6.05	3.92	4.46	4.29	5.67	5.08
f_u (%) mouse/human	3.8/3.6	2.1/3.9	0.1/0.4	4.7/9.4	4.2/5.6	6.8/10.3	0.3/0.5	1.7/1.8
THP-1 IC/EC	26	44	140	25	31	23	126	93
CYP3A4 induction @ 1 and 10 μM	33.4/42.7	8.2/14.1	6.2/1.7	0.8/7.9	1.6/1.7	1.6/2.7	1.1/2.4	1.3/1.3
Metabolite‡/parent ratio in microsomes (without/with NADPH)	1.3/0.5	Met. n.d.	Met. n.d.	n.d.	Met. n.d.	Met. n.d.	Met. n.d.	Met. n.d./0.2
HepG2 CC_{50}/MIC	154	2,080	4,133	4,556	2,225	1,743	273	823

*_M. abscessus_ subsp _abscessus_ ATCC19977 was used in all potency assays unless specified otherwise.
†cLogP values were calculated using ChemDraw (version 22.2.0.3300).
‡Product of deacylation or decarbamoylation at C25. n.d.: not detected.
ssMIC: serum-shifted MIC; Mtb: _M. tuberculosis_ H37Rv; $MacIC_{50}$: concentration that inhibits growth of intracellular Mab in THP-1 macrophages by 50%; casMBC: minimum bactericidal activity against nonreplicating Mab in caseum surrogate; f_u: fraction unbound; V_d: volume of distribution; CL: clearance; MW: molecular weight; THP-1 IC/EC: intracellular to extracellular concentration ratio in THP-1 derived macrophages; CC_{50}: cytotoxic concentration causing 50% cell death; n.d. not determined; Met. n.d.: metabolite not detected.

identical *M. tuberculosis* MICs for RBT and the prioritized leads (Table 1). Thus, the C25-substituted rifamycins hold promise not only for Mab-PD but also for TB by eliminating the drug–drug interaction liability typical of rifamycins.

RBT undergoes extensive hepatic metabolism. One of its major metabolites is the deacylation product at C25. To examine the stability of the ester or carbamate groups appended at C25 in the RBT analogs, we measured their metabolic stability in human liver microsomes, contributing to clearance in humans. The assays were set up with and without NADPH as cofactor, to probe phase I metabolism as well as noncytochrome P450-mediated metabolism (esters are among functional groups susceptible to non-NADPH-mediated metabolism). Deacylation and decarbamoylation products were quantified at regular intervals up to 60 min. RBT was effectively deacetylated both in the absence and presence of NADPH, reaching metabolite/parent ratios of 1.3 and 0.5 at 60 min, without and with NADPH, respectively. No deacyl- or decarbamoyl-metabolites were detected for any of the leads in the absence of NADPH. With NADPH, only UMN-132 released detectable amounts of decarbamoylation product, with a metabolite/parent ratio of 0.2 at 60 min (Table 1 and *SI Appendix*, Table S1). Thus, the rifamycin leads are less metabolically labile than RBT in human liver microsomes.

To further discriminate the lead compounds and identify potential determinants of cytotoxicity, we measured the CC_{50} (concentrations causing 50% cell death) of the rifamycins in the conventional HepG2 cell line, compared to RBT. We found CC_{50} ranging from 14 to 175 μM, generally lower than RBT which has a CC_{50} of 170 μM. As cLogP increased, CC_{50} generally decreased, and this was also correlated with higher partitioning into THP-1 macrophages (Fig. 2*B*). However, CC_{50}/MIC ratios, an indirect measure of selectivity, were higher than RBT for all compounds tested, from 273 to 4,556 for the lead compounds, while the measured CC_{50}/MIC of RBT was 154 (Table 1 and Dataset S1).

Efficacy of the Selected Leads in the GM-CSF Knockout Mouse Model of Acute Infection. To differentiate the selected lead compounds based on in vivo efficacy, we searched for a mouse model that offers robust and reproducible growth, and a wide dynamic range. We settled on the GM-$CSF^{-/-}$ model of

Table 2. Impact of nonspecific binding to human serum on Mab growth inhibition by the rifamycins

compound	IC_{50} in CAMHB (μM)	IC_{50} in 1:1 CAMH-B:hSerum (μM)	IC_{50} serum shift (−fold)	"active" fraction (%)*	plasma f_u (%, human)
OPC-167832	0.12	17.5	147.5	0.61	1.22
RBT	1.2	9.7	8.1	12.35	3.84
UMN-7	0.052	0.93	17.9	5.59	0.09
UMN-15	0.01	0.12	12.0	8.33	0.19
UMN-20	0.062	1.6	25.8	3.88	0.03
UMN-22	0.031	0.15	4.8	20.67	3.86
UMN-34	0.018	0.15	8.3	12.00	0.43
UMN-46	0.017	0.048	2.8	35.42	9.41
UMN-64	0.10	0.26	2.6	38.46	7.36
UMN-67	0.039	0.54	13.8	7.22	3.23
UMN-92	0.062	0.36	5.8	17.22	13.40
UMN-120	0.018	0.045	2.5	40.00	5.62
UMN-121	0.028	0.050	1.8	56.00	10.30
UMN-123	0.018	0.14	7.8	12.86	0.54
UMN-125	0.016	0.21	13.1	7.62	0.76
UMN-131	0.06	0.20	3.3	30.00	6.55
UMN-132	0.013	0.070	5.4	18.57	1.84
UMN-133	0.036	0.16	4.4	22.50	3.11

*The "active" fraction (f_A) was inferred from the serum shift (ss) as follows: f_A = (1/ss) × 100 in %.
IC_{50}: concentration that inhibits growth of Mab type strain ATCC19977 by 50%; CAMHB: cation adjusted Mueller–Hinton broth devoid of plasma proteins; hSerum: human serum; f_u: fraction unbound.

intratracheal infection (22) as the best available option (21). We selected six rifamycins that combined either attractive AUC/MIC (total and/or corrected for nonspecific binding) or high uptake into macrophages, with low to no CYP3A4 induction.

GM-CSF$^{-/-}$ mice were infected via the intratracheal route for 2 d, after which therapy was initiated and administered daily for 7 d. To optimize the probability of observing an RBT effect even if marginal, a dose of 25 mg/kg was selected, more than doubling the human-equivalent dose of 300 mg or 10 mg/kg in mice. All rifamycin analogs were dosed orally at 25 mg/kg except UMN-123 and UMN-132, which were given at 12.5 mg/kg to ensure optimal tolerability given their relatively high plasma AUC, long half-life, high partitioning into macrophages and slightly lower selectivity index (CC_{50}/MIC) (Table 1). At the selected doses, all analogs achieved excellent AUC/(ss)MIC (Table 1 and Dataset S2). All compounds were well tolerated with no weight loss or signs of discomfort and were significantly more efficacious than RBT, which neither reduced lung burden nor prevented bacterial growth over the 7-d therapy duration in this model, despite the higher-than-standard dose. We observed a wide range of efficacy, from approximately 2-log reduction in lung burden compared to untreated mice at the end of therapy (UMN-22, UMN-34, and UMN-123) to more than a 2-log reduction compared to the start of treatment or pronounced bactericidal effect for UMN-120 and UMN-121, which reduced the bacterial burden below the limit of detection (Fig. 4*A*). Peak and trough plasma samples were collected on the last day of treatment to measure rifamycin concentrations and ensure on-target exposure.

To put these promising results into perspective, we also measured the efficacy of a typical standard-of-care intensive drug regimen (PATIENCE trial NCT02419989) composed of amikacin and imipenem as injectables combined with oral clofazimine and tedizolid, at the human equivalent doses of 50 mg/kg via subcutaneous (SC) injection once daily (QD), 50 mg/kg twice daily via

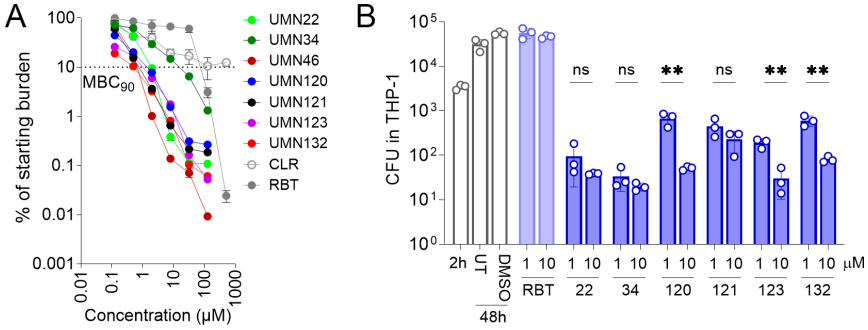

Fig. 3. Bactericidal activity of the frontrunners against nonreplicating Mab in caseum surrogate (*A*) and intracellular Mab ATCC19977 in THP-1-derived macrophages (*B*). (*A*) The CFU/mL caseum are expressed in percent of starting burden, with MBC_{90} indicating 90% kill over a 5-d treatment duration. Clarithromycin (CLR) was used as control and RBT as the rifamycin comparator. (*B*) Drug treatment was initiated 2 h post infection for 48 h, at 1 and 10 μM. Assays were carried out in technical triplicates. In all 1- and 10-μM treatment groups with RBT analogs, intracellular bacterial burden was significantly lower than prior to treatment initiation (2 h), indicating bactericidal activity (one-way ANOVA with Dunnett's posttest, all *P* values < 0.0001 **** not shown for clarity). Dose–response was queried by comparing the 1- and 10-μM treatment groups using Student's *t* test. ns: not significant, **: *P* < 0.01. UT: untreated; DMSO: vehicle only.

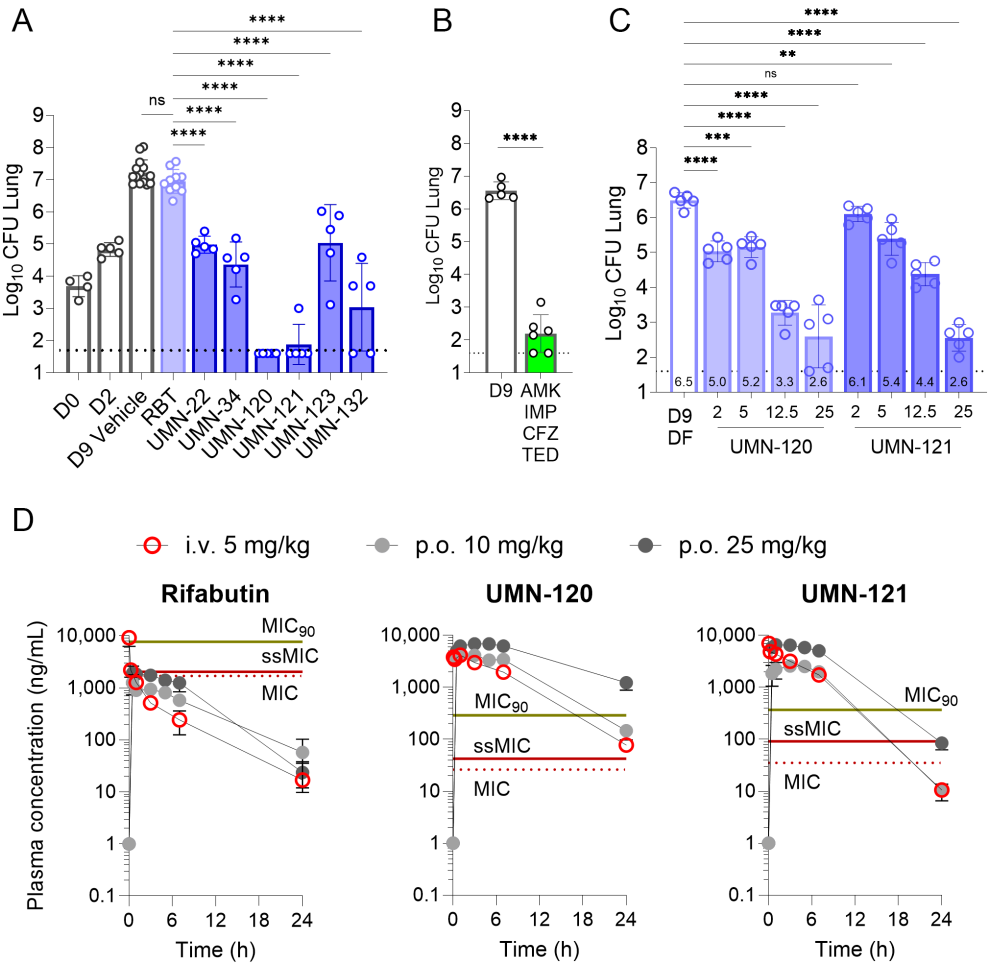

Fig. 4. Efficacy of the selected rifamycin leads in the GM-CSF$^{-/-}$ mouse model of acute Mab infection and PK-PD profiles of the preclinical development candidates. (*A*) Reduction of lung CFU in GM-CSF$^{-/-}$ mice following seven oral daily doses administered between Day 2 and Day 9 (D2, D9) at 25 mg/kg except UMN-123 and UMN-132 given at 12.5 mg/kg. LOD: limit of detection or 1.6 log CFU. (*B*) Efficacy of a typical intensive phase drug combination (amikacin AMK, imipenem IMP, clofazimine CFZ, and tedizolid TED) administered for 7 d at human-equivalent doses. (*C*) Dose–response efficacy of the selected PDCs UMN-120 and UMN-121 from 2 to 25 mg/kg as indicated. D9 DF: Drug-free arm on D9 after seven daily doses. Numbers at the bottom of each column are mean Log CFU/mouse (n = 5). (*D*) Plasma concentration–time profiles of RBT and the two preclinical development candidates in CD-1 mice following administration as indicated, compared to key potency values; dotted red line: MIC against Mab ATCC19977, solid red line: serum-shifted MIC; green line: MIC_{90} or minimum concentration that inhibits growth of 90% of clinical isolates (n = 76).

SC injection, 12.5 mg/kg QD orally, and 10 mg/kg QD orally, respectively. In this model, UMN-120 and UMN-121 at 25 mg/kg were at least as effective as the four-drug regimen in reducing lung bacterial burden over 7 d (Fig. 4*B*). To identify the minimum efficacious dose for these two compounds, we treated *M. abscessus*–infected GM-CSF$^{-/-}$ mice with a range of daily doses and determined that 2 mg/kg UMN-120 and 5 mg/kg UMN-121 both achieved a statistically significant >1 log CFU reduction of lung burden. CFU reduction was generally proportional to dose (Fig. 4*C*). We also performed pharmacokinetic studies in naive mice at the same doses and observed that the area under the concentration–time curve (AUC) over the MIC was a consistent driver of efficacy (*SI Appendix*, Fig. S4). Finally, we superimposed key potency values onto the plasma concentration–time profiles of RBT and the two best performing rifamycins, showing that plasma concentrations of UMN-120 and UMN-121 following an oral 25 mg/kg dose remain above the standard MIC and the serum-shifted MIC for the entire dosing interval. In addition, plasma concentrations were above the MIC_{90} (minimum concentration that inhibits growth of 90% of clinical isolates, n = 76, dataset S3) for most of the dosing interval (Fig. 4*D*). In contrast, RBT at 25 mg/kg (approximately twofold the human equivalent dose) did not achieve therapeutic concentrations.

Considering these impressive efficacy results together with bactericidal activity against nonreplicating persisters in caseum, CYP3A4 induction data and selectivity indices (Table 1), UMN-120 and UMN-121 were selected as preclinical development candidates (PDCs) for in-depth biological profiling.

Extensive Biological Profiling of the Proposed PDCs. To quantify the bactericidal activity of the two PDCs compared to RBT, we generated time– and concentration–kill curves at multiples of their respective MICs (0.5× to 8×), where MICs were 1.4 μM for RBT and 0.03 μM for the PDCs. In the lower part of the concentration range (0.5× to 2× MIC) we observed increased killing activity, which gradually tapered off to reach a plateau of approximately 2-log kill at the highest concentration of 8× MIC. This was true for RBT and the PDCs, proportional to the ~50-fold difference in absolute MIC (Fig. 5*A* and *SI Appendix*, Fig. S5).

PAE is the delayed regrowth of bacteria following brief antibiotic exposure, and a strong PAE may contribute to effective suppression of bacterial growth between clinical doses when plasma concentrations fall below the MIC (34). Strong PAE is an attractive feature of rifamycins in *M. tuberculosis* (35, 36). *M. abscessus* ATCC 19977 regrowth was measured over a period of 3 d, after a brief exposure to RBT and the PDCs at 1 to 8× MIC, showing

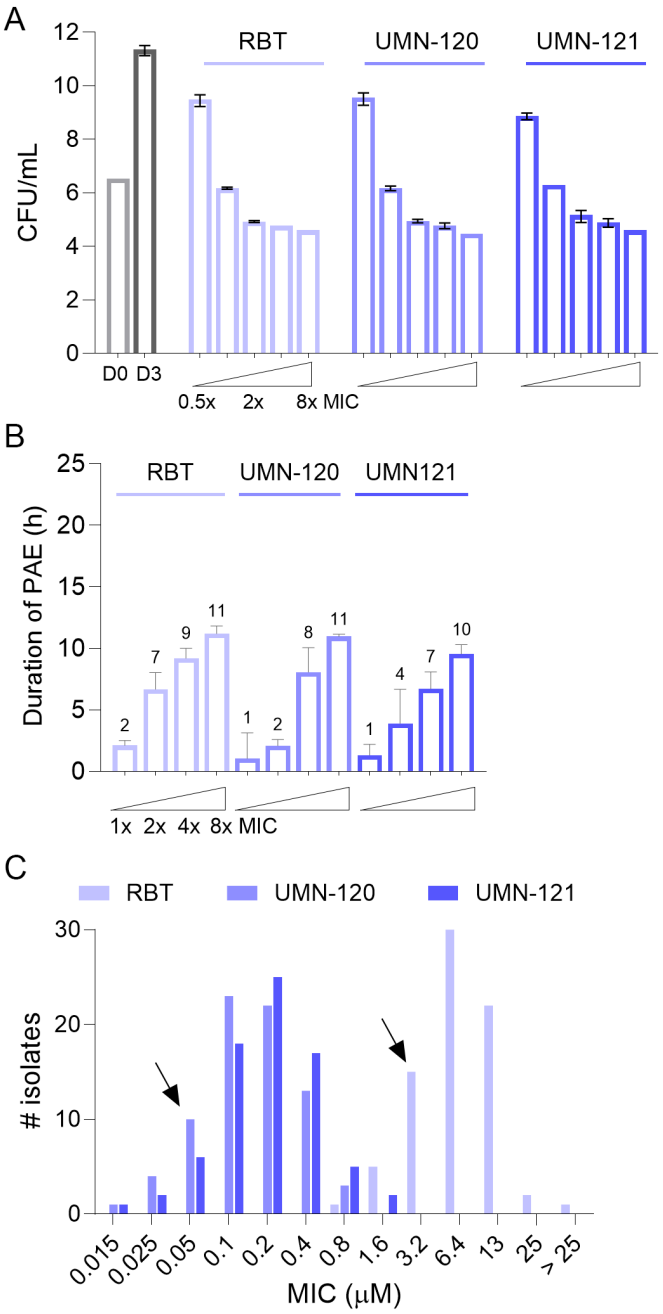

Fig. 5. Extensive microbiological profiling of the PDCs. (*A*) Dose–response bactericidal activity in replicating cultures at multiples of the MIC against the type strain ATCC19977, measured after 3 d (D3) of incubation. (*B*) Post-antibiotic effect (PAE) of RBT and the PDCs at multiples of their respective MICs. (*C*) MIC distributions of RBT and the PDCs against a panel of 76 *M. abscessus* clinical isolates. The arrows indicate the position of the *M. abscessus* subsp. *abscessus* type strain ATCC19977.

concentration-proportional PAE from 1 to 2 h at 1× MIC to 10 to 11 h at 8× MIC for the three compounds (Fig. 5*B*), twofold to threefold the generation time of Mab (~4 h) thus confirming the attractive PAE of the class.

To confirm on-target mechanism of action, we selected spontaneous resistant mutants to RBT, UMN-120, and UMN-121 on solid medium containing 4× their respective MIC. The frequency of resistance to the three compounds was similar, at 2.6×10^{-8}, 7.7×10^{-8}, and 1.3×10^{-8}, respectively. We selected five mutants resistant to each of UMN-120 and UMN-121 and subjected them to targeted sequencing of the *rpoB* gene. All 10 mutants returned mutations commonly found in the rifampicin resistance determining region (RRDR): H447Y (n = 3) and S452L (n = 7).

Although the RpoB target is epidemiologically conserved, the Mab complex presents extensive genomic diversity, as seen in all nontuberculous mycobacteria. To gauge the clinical potential of the series against a wide range of clinical isolates, we measured the MICs of the PDCs against 76 strains covering the 3 Mab subspecies. We found MIC_{50} and MIC_{90} of 0.10 and 0.31 μM for UMN-120, 0.13 and 0.40 μM for UMN-121, and 4.7 and 9.1 μM for RBT, respectively (Fig. 5*C* and Dataset S3). Overall, the MIC_{90} were within 10-fold of the MIC against the Mab ATCC19977 type strain and achieved in mice throughout the dosing interval at the efficacious and tolerated dose of 25 mg/kg (Fig. 4*D*).

Discussion

We have found C25-substituted RBT analogs that block intrabacterial ADP ribosylation, exhibit much reduced CYP3A4 induction and improved metabolic stability compared to RBT. The lead optimization campaign described here has delivered two preclinical candidates that reduced the starting bacterial burden by more than 3 log after only 7 d of daily oral therapy. In prior work, we showed that this compound series is active in vitro against Arr-positive rapid- and slow-growing *Mycobacterium fortuitum*, *Mycobacterium chelonae* and *Mycobacterium simiae*, expanding the spectrum of optimized rifabutin analogs beyond Mab (37). Importantly, most analogs are as potent as RBT against (Arr-negative) *M. tuberculosis* and may thus offer clinical utility for TB patients with comorbidities requiring treatment with CYP3A4 substrates such as antiretroviral agents and CFTR modulators.

We previously described C25-substituted esters (15) that block intrabacterial ribosylation. In this expanded lead optimization, five of the seven prioritized candidates are carbamate derivatives (Fig. 1) that offer several advantages over esters: lack of CYP3A4 induction, superior PK-PD properties and therefore best in vivo efficacy.

While UMN-120 consistently showed highest AUC/MIC, AUC/ssMIC, and *f*AUC/MIC resulting in highest reduction of mouse lung burden, we did not identify a single PK-PD parameter that correlates with efficacy across the series. It is likely that a composite signature—integrating several potency parameters and site-of-disease PK—drives efficacy and that this signature is mouse model dependent. A limitation of the present work is the lack of an assay that measures potency against Mab in biofilm-like structures. Many such assays have been described, featuring varying growth conditions and readouts, and often delivering discrepant potency values for individual antibiotics (38). Validation of a clinically relevant and predictive assay is needed prior to integrating activity against Mab in biofilms into the composite PK-PD signature mentioned above.

Our results are consistent with the concept of a sweet spot of hydrophobicity for the class: too little may negatively affect tissue distribution and uptake by infected cells, whereas too much reduces the active fraction, and may lead to detrimental tissue accumulation increasing the potential for toxicity. Surprisingly, UMN-120 and UMN-121, the most efficacious analogs, display a low volume of distribution following intravenous administration to uninfected mice (Table 1). They do not significantly activate the human PXR, which controls not only CYP3A4 expression but also induces the host's P-glycoprotein (Pgp) efflux pump and other efflux effectors. Indeed, PXR was shown to modulate macrophage drug-efflux transporter expression and activity, which compromised the anti-TB efficacy of rifampicin in vitro and in mice (39). It is thus possible that UMN-120 and UMN-121 do not promote

drug extrusion out of infected macrophages, unlike rifampicin (40), and accumulate precisely where the pathogen resides.

The efficacy of RBT in Mab infected mice is model-dependent (41), which likely extends to the analogs described here. Current efforts focus on identifying the minimum efficacious dose to investigate the reduction of lung burden in several models of chronic Mab infection including models that feature necrotic lesions. We have selected UMN-120 and UMN-121 as promising compounds across mouse models and in patients not only on the basis of their excellent efficacy in the GM-CSF$^{-/-}$ model but also for their strong bactericidal activity in replicating cultures and against nonreplicating persisters in caseum surrogate (Table 1). We anticipate that these properties will be key drivers of efficacy in necrotic lesions.

Rifamycins, like β-lactams and fluoroquinolones, are a major class of antibiotics with a long history of clinical use against a wide range of bacterial infections. But unlike β-lactams and fluroquinolones for which 2nd, 3rd, and 4th generation derivatives have been the focus of extensive discovery and development efforts, redesign of rifamycins to better target select pathogens has not met with much success. The present work constitutes a first step towards the development of 2nd generation rifamycins with improved efficacy against mycobacterial infections.

Methods

Impact of Human Serum on Potency. To calculate the Mab MIC corrected for nonspecific binding to plasma proteins, MICs were measured in cation-adjusted Mueller–Hinton broth (CAMHB, free of bovine serum albumin) and in CAMHB supplemented with human serum in a 1:1 ratio. Concentrations that inhibit growth by 50% (IC_{50}) are reported and were used to infer the MIC shift, as they are more reproducible than IC_{90} due to the limited growth of Mab in CAMHB/human serum. The assays were carried out twice and mean values are reported.

PAE. The PAE was determined as previously described with several modifications (42). 14 mL vented round-bottom tubes containing the desired rifamycin concentration in Middlebrook 7H9 broth were inoculated with exponentially growing *M. abscessus* subsp. *abscessus* ATCC 19977 at a starting OD_{600} of 0.2. The tubes were incubated at 37 °C for 4 h. Cultures were washed two times, via centrifugation and resuspension of the cell pellets in Middlebrook 7H9, and incubated at 37 °C for 3 d, with shaking on an orbital shaker. At selected timepoints, aliquots were sampled to monitor OD_{600} using a 96-well flat, clear bottom, Costar cell culture plate and the Infinite 200 Pro plate reader. The duration of the PAE was calculated as the time taken for the drug-treated culture to reach 50% of the maximum OD_{600} of the drug-free culture minus the time taken for the drug-free control to reach the same point (43).

Efficacy Evaluation in the GM-CSF KO Mouse Model. Efficacy studies were approved by the IACUC of Colorado State University. In vivo efficacy determinations were carried out as described previously (22, 44), with several modifications, in GM-CSF KO (B6.129S-Csf2tm1Mlg/J) mice which were bred at Colorado State University animal housing facilities from strain #:026812 of Jackson Laboratories. The mice were infected with *M. abscessus* subsp. *abscessus* ATCC 19977 (~10^4 CFU/animal) via intratracheal delivery using a microsprayer device. Two days postinfection, groups of five to six mice received the study compounds, RBT or the vehicle once daily for seven consecutive days by oral gavage. Rifamycins were formulated in 0.5% carboxymethylcellulose and 0.5% Tween 80 in water. Amikacin, imipenem, clofazimine, and tedizolid were administered at the human equivalent doses of 50 mg/kg via subcutaneous (SC) injection once daily (QD) in 0.9% Saline, 50 mg/kg twice daily via SC injection in D5W, 12.5 mg/kg QD orally in 5% gum arabic, and 10 mg/kg QD orally in 5% Gum Arabic, respectively. The doses and dosing frequencies were determined through PK studies in CD-1 mice to reproduce published human PK parameters (45–49) within the limits of feasibility and tolerability, and accounting for drug–drug interactions when dosed in combination. Clofazimine was administered in the evening with the second dose of imipenem. Twenty-four hours after the last dose, the lungs were harvested and homogenized in sterile PBS and bacterial load was determined by plating serial dilutions of organ homogenates onto Middlebrook 7H11 agar (BD) supplemented with 0.2% (vol/vol) glycerol, 10% (vol/vol) OADC, and 0.4% (wt/vol) activated charcoal. The plates were incubated for 3 to 5 d at 37 °C prior to CFU enumeration. The data were analyzed using one-way ANOVA with Dunnett's multiple comparison test (GraphPad Prism v10).

Data, Materials, and Software Availability. All study data are included in the article and/or supporting information.

ACKNOWLEDGMENTS. This work was funded by NIH-NIAID awards R01 AI177342 (T.D. and C.C.A.), U19AI142731, R01AI132374, and Cystic Fibrosis Foundation award DICK24XX0 (V.D and T.D.), the Deutsche Forschungsgemeinschaft (DFG, German Research Foundation) award 432291016, and Mukoviszidose Institut gGmbH project no. 2202 (Bonn, Germany), the research and development arm of the German Cystic Fibrosis Association Mukoviszidose e. V. (A.R.).

Author affiliations: [a]Center for Discovery and Innovation, Hackensack Meridian Health, Nutley, NJ 07110; [b]Department of Medical Sciences, Hackensack Meridian School of Medicine, Nutley, NJ 07110; [c]Department of Medicinal Chemistry, College of Pharmacy, University of Minnesota, Minneapolis, MN 55455; [d]Mycobacteria Research Laboratories, Department of Microbiology, Immunology and Pathology, Colorado State University, Fort Collins, CO 80523; [e]Institut für Pharmazie, Martin-Luther-Universität Halle-Wittenberg, Halle (Saale) 06120, Germany; and [f]Department of Microbiology and Immunology, Georgetown University, Washington, DC 20057

Author contributions: V.D., T.L., M.J., W.W., A.R., P.I., J.P., M.Z., M.G.-J., C.C.A., and T.D. designed research; T.L., C.F.W., J.P.S., D.C.J., I.M.A., H.L., S.R., M.X., M.S.-O., N.C.D., K.K., J. Schmitt, L.M., J. Sarathy, F.K., S.P., B.T., C.F., and J.P. performed research; V.D., T.L., M.J., W.W., and M.G.-J. analyzed data; C.C.A. and T.D. provided funding; and V.D. wrote the paper.

1. B. Prideaux *et al.*, The association between sterilizing activity and drug distribution into tuberculosis lesions. *Nat. Med.* **21**, 1223–1227 (2015).
2. M. Xie *et al.*, ADP-ribosylation-resistant rifabutin analogs show improved bactericidal activity against drug-tolerant *M. abscessus* in caseum surrogate. *Antimicrob. Agents. Chemother.* **67**, e0038123 (2023), 10.1128/aac.00381-23.
3. W. Fox, G. A. Ellard, D. A. Mitchison, Studies on the treatment of tuberculosis undertaken by the British Medical Research Council tuberculosis units, 1946–1986, with relevant subsequent publications. *Int. J. Tuberc. Lung Dis.* **3**, S231–279 (1999).
4. A. Loeliger *et al.*, Protease inhibitor-containing antiretroviral treatment and tuberculosis: Can rifabutin fill the breach? *Int. J. Tuberc Lung Dis.* **16**, 6–15 (2012).
5. S. E. Dorman *et al.*, Four-month rifapentine regimens with or without moxifloxacin for tuberculosis. *N. Engl. J. Med.* **384**, 1705–1718 (2021).
6. WHO, *WHO Consolidated Guidelines on Tuberculosis: Module 1: Prevention: Tuberculosis Preventive Treatment* (World Health Organization, Geneva, 2020).
7. S. Luthra, A. Rominski, P. Sander, The role of antibiotic-target-modifying and antibiotic-modifying enzymes in mycobacterium abscessus drug resistance. *Front. Microbiol.* **9**, 2179 (2018).
8. U. S. Ganapathy *et al.*, Blocking bacterial naphthohydroquinone oxidation and ADP-ribosylation improves activity of rifamycins against *Mycobacterium abscessus*. *Antimicrob. Agents Chemother.* **65**, e0097821 (2021).
9. K. Koteva *et al.*, Rox, a rifamycin resistance enzyme with an unprecedented mechanism of action. *Cell Chem. Biol.* **25**, 403–412.e5 (2018).
10. E. A. Campbell *et al.*, Structural mechanism for rifampicin inhibition of bacterial RNA polymerase. *Cell* **104**, 901–912 (2001).
11. J. Baysarowich *et al.*, Rifamycin antibiotic resistance by ADP-ribosylation: Structure and diversity of Arr. *Proc. Natl. Acad. Sci. U.S.A.* **105**, 4886–4891 (2008).
12. S. Quan, H. Venter, E. R. Dabbs, Ribosylative inactivation of rifampin by Mycobacterium smegmatis is a principal contributor to its low susceptibility to this antibiotic. *Antimicrob. Agents Chemother.* **41**, 2456–2460 (1997).
13. A. Rominski, A. Roditscheff, P. Selchow, E. C. Bottger, P. Sander, Intrinsic rifamycin resistance of Mycobacterium abscessus is mediated by ADP-ribosyltransferase MAB_0591. *J. Antimicrob. Chemother.* **72**, 376–384 (2017).
14. L. Paulowski *et al.*, C25-modified rifamycin derivatives with improved activity against *Mycobacterium abscessus*. *PNAS Nexus* **1**, pgac130 (2022).
15. T. Lan *et al.*, Redesign of rifamycin antibiotics to overcome ADP-ribosylation-mediated resistance. *Angew. Chem. Int. Ed Engl.* **61**, e202211498 (2022).
16. C. C. Aldrich, T. Lan, T. Dick, U. Ganapathy, V. Dartois, "Rifamycins for nontuberculous mycobacteria." PCT/US2023/034573 (2023).
17. F. Saluzzo *et al.*, CFTR modulator therapies: Potential impact on airway infections in cystic fibrosis. *Cells* **11**, 1243 (2022).
18. M. Smith *et al.*, Ivacaftor-elexacaftor-tezacaftor and tacrolimus combination in cystic fibrosis. *J. Cyst. Fibros* **21**, e8–e10 (2022).
19. A. M. Baciewicz, C. R. Chrisman, C. K. Finch, T. H. Self, Update on rifampin, rifabutin, and rifapentine drug interactions. *Curr. Med. Res. Opin.* **29**, 1–12 (2013).
20. S. R. Ashkar *et al.*, Optimization of benzoxazinorifamycins to minimize hPXR activation for the treatment of tuberculosis and HIV coinfection. *ACS Infect Dis.* **8**, 1408–1421 (2022).

21. V. Dartois *et al.*, Preclinical murine models for the testing of antimicrobials against Mycobacterium abscessus pulmonary infections: Current practices and recommendations. *Tuberculosis (Edinb)* **147**, 102503 (2024).
22. M. A. De Groote *et al.*, GM-CSF knockout mice for preclinical testing of agents with antimicrobial activity against *Mycobacterium abscessus*. *J. Antimicrob. Chemother.* **69**, 1057–1064 (2014).
23. N. T. Lan *et al.*, Randomised pharmacokinetic trial of rifabutin with lopinavir/ritonavir-antiretroviral therapy in patients with HIV-associated tuberculosis in Vietnam. *PLoS One* **9**, e84866 (2014).
24. T. Schon *et al.*, Rifampicin-resistant and rifabutin-susceptible *Mycobacterium tuberculosis* strains: A breakpoint artefact? *J. Antimicrob. Chemother.* **68**, 2074–2077 (2013).
25. Z. Yan *et al.*, Introducing the dynamic well-stirred model for predicting hepatic clearance and extraction ratio. *J. Pharm. Sci.* **113**, 1094–1112 (2024), 10.1016/j.xphs.2023.12.020.
26. Z. Yan *et al.*, New methodology for determining plasma protein binding kinetics using an enzyme reporter assay coupling with high-resolution mass spectrometry. *Anal. Chem.* **95**, 4086–4094 (2023).
27. R. Dawson *et al.*, Quabodepistat in combination with delamanid and bedaquiline in participants with drug-susceptible pulmonary tuberculosis: protocol for a multicenter, phase 2b/c, open-label, randomized, dose-finding trial to evaluate safety and efficacy. *Trials* **25**, 70 (2024).
28. G. T. Robertson *et al.*, Comparative analysis of pharmacodynamics in the C3HeB/FeJ mouse tuberculosis model for DprE1 inhibitors TBA-7371, PBTZ169, and OPC-167832. *Antimicrob. Agents Chemother.* **65**, e0058321 (2021).
29. J. P. Sarathy, M. D. Zimmerman, M. Gengenbacher, V. Dartois, T. Dick, *Mycobacterium tuberculosis* DprE1 inhibitor OPC-167832 is active against *Mycobacterium abscessus* in vitro. *Antimicrob. Agents Chemother.* **66**, e0123722 (2022).
30. B. R. Kim, B. J. Kim, Y. H. Kook, B. J. Kim, Mycobacterium abscessus infection leads to enhanced production of type 1 interferon and NLRP3 inflammasome activation in murine macrophages via mitochondrial oxidative stress. *PLoS Pathog.* **16**, e1008294 (2020).
31. A. Bernut, J. L. Herrmann, D. Ordway, L. Kremer, The diverse cellular and animal models to decipher the physiopathological traits of *Mycobacterium abscessus* infection. *Front. Cell Infect. Microbiol.* **7**, 100 (2017).
32. D. B. Aziz *et al.*, Rifabutin is active against *Mycobacterium abscessus* complex. *Antimicrob. Agents. Chemother.* **61**, e00155-17 (2017).
33. Department of Health and Human Services, Center for Drug Evaluation and Research (CDER), FDA, In Vitro Drug Interaction Studies–Cytochrome P450 Enzyme- and Transporter-Mediated Drug Interactions Guidance for Industry (2020). https://collections.nlm.nih.gov/catalog/nlm:nlmuid-101767646-pdf. Accessed 15 April 2025.
34. W. A. Craig, Post-antibiotic effects in experimental infection models: relationship to *in-vitro* phenomena and to treatment of infections in man. *J. Antimicrob. Chemother.* **31**, 149–158 (1993).
35. C. Y. Chan, C. Au-Yeang, W. W. Yew, C. C. Leung, A. F. Cheng, In vitro postantibiotic effects of rifapentine, isoniazid, and moxifloxacin against *Mycobacterium tuberculosis*. *Antimicrob. Agents Chemother.* **48**, 340–343 (2004).
36. C. Y. Chan, C. Au-Yeang, W. W. Yew, M. Hui, A. F. Cheng, Postantibiotic effects of antituberculosis agents alone and in combination. *Antimicrob. Agents Chemother.* **45**, 3631–3634 (2001).
37. U. S. Ganapathy, T. Lan, V. Dartois, C. C. Aldrich, T. Dick, Blocking ADP-ribosylation expands the anti-mycobacterial spectrum of rifamycins. *Microbiol. Spectr.* **11**, e0190023 (2023).
38. H. M. Meliefste, S. E. Mudde, N. C. Ammerman, J. E. M. de Steenwinkel, H. I. Bax, A laboratory perspective on Mycobacterium abscessus biofilm culture, characterization and drug activity testing. *Front. Microbiol.* **15**, 1392606 (2024).
39. E. Bhagyaraj *et al.*, A human xenobiotic nuclear receptor contributes to nonresponsiveness of *Mycobacterium tuberculosis* to the antituberculosis drug rifampicin. *J. Biol. Chem.* **293**, 3747–3757 (2018).
40. K. N. Adams *et al.*, Drug tolerance in replicating mycobacteria mediated by a macrophage-induced efflux mechanism. *Cell* **145**, 39–53 (2011).
41. V. Dartois, T. Dick, Toward better cures for *Mycobacterium abscessus* lung disease. *Clin. Microbiol. Rev.* **37**, e0008023 (2024), 10.1128/cmr.00080-23.
42. R. Zhu *et al.*, *In vitro* and intracellular inhibitory activities of nosiheptide against *Mycobacterium abscessus*. *Front. Microbiol.* **13**, 926361 (2022).
43. M. I. Islam *et al.*, In vitro activity of DNF-3 against drug-resistant *Mycobacterium tuberculosis*. *Int. J. Antimicrob. Agents* **54**, 69–74 (2019).
44. S. E. Maloney *et al.*, Spray dried tigecycline dry powder aerosols for the treatment of Nontuberculous mycobacterial pulmonary infections. *Tuberculosis (Edinb)* **139**, 102306 (2023).
45. M. Staneva, B. Markova, I. Atanasova, D. Terziivanov, Pharmacokinetic and pharmacodynamic approach for comparing two therapeutic regimens using amikacin. *Antimicrob. Agents Chemother.* **38**, 981–985 (1994).
46. A. J. Lepak *et al.*, Development of modernized acinetobacter baumannii susceptibility test interpretive criteria for recommended antimicrobial agents using pharmacometric approaches. *Antimicrob. Agents Chemother.* **67**, e0145222 (2023).
47. D. N. Fish, I. Teitelbaum, E. Abraham, Pharmacokinetics and pharmacodynamics of imipenem during continuous renal replacement therapy in critically ill patients. *Antimicrob. Agents Chemother.* **49**, 2421–2428 (2005).
48. M. T. Abdelwahab *et al.*, Clofazimine pharmacokinetics in patients with TB: Dosing implications. *J. Antimicrob. Chemother.* **75**, 3269–3277 (2020).
49. A. Y. J. Park *et al.*, Pharmacokinetics of tedizolid in plasma and sputum of adults with cystic fibrosis. *Antimicrob. Agents Chemother.* **62**, e00550-18 (2018).